Simulation domain size requirements for elastic response of 3D polycrystalline materials

2016 Modelling Simul. Mater. Sci. Eng. 24 015006

(http://iopscience.iop.org/0965-0393/24/1/015006)

IOP Publishing Modelling and Simulation in Materials Science and Engineering

Modelling Simul. Mater. Sci. Eng. **24** (2016) 015006 (13pp) doi:10.1088/0965-0393/24/1/015006

Simulation domain size requirements for elastic response of 3D polycrystalline materials

Tugce Ozturk[1], Clayton Stein[1], Reeju Pokharel[1,2], Christopher Hefferan[3,4], Harris Tucker[1], Sushant Jha[5], Reji John[6], Ricardo A Lebensohn[2], Peter Kenesei[7], Robert M Suter[3] and Anthony D Rollett[1]

[1] Carnegie Mellon University, Department of Materials Science and Engineering, 5000 Forbes Avenue, Pittsburgh, PA 15213, USA
[2] Materials Science and Technology Division, Los Alamos National Laboratory, Los Alamos, NM 87544, USA
[3] Carnegie Mellon University, Department of Physics, 5000 Forbes Avenue, Pittsburgh, PA 15213, USA
[4] RJ Lee Group, 350 Hochberg Road, Monroeville, PA 15146, USA
[5] Universal Technology Corporation, Dayton, OH 45432, USA
[6] Air Force Research Laboratory, Materials & Manufacturing Directorate, Wright-Patterson AFB, OH 45433–7817, USA
[7] Advanced Photon Source, Argonne National Laboratory, 9700 South Cass Avenue, Lemont, IL 60439, USA

E-mail: tozturk@andrew.cmu.edu

Received 9 April 2015, revised 17 August 2015
Accepted for publication 20 October 2015
Published 27 November 2015

Abstract

A fast Fourier transform (FFT) based spectral algorithm is used to compute the full field mechanical response of polycrystalline microstructures. The field distributions in a specific region are used to determine the sensitivity of the method to the number of surrounding grains through quantification of the divergence of the field values from the largest simulation domain, as successively smaller surrounding volumes are included in the simulation. The analysis considers a mapped 3D structure where the location of interest is taken to be a particular pair of surface grains that enclose a small fatigue crack, and synthetically created statistically representative microstructures to further investigate the effect of anisotropy, loading condition, loading direction, and texture. The synthetic structures are generated via DREAM3D and the measured material is a cyclically loaded, Ni-based, low solvus high refractory (LSHR) superalloy that was characterized via 3D high energy x-ray diffraction microscopy (HEDM). Point-wise comparison of distributions in

the grain pairs shows that, in order to obtain a Pearson correlation coefficient larger than 99%, the domain must extend to at least the third nearest neighbor. For an elastic FFT calculation, the stress–strain distributions are not sensitive to the shape of the domain. The main result is that convergence can be specified in terms of the number of grains surrounding a region of interest.

Keywords: spectral full-field modeling, fast Fourier transform algorithm, anisotropic elastic response, microstructures, high-energy x-ray diffraction microscopy, representative volume element

(Some figures may appear in colour only in the online journal)

1. Introduction

For small deformations of most polycrystalline materials, a linear relationship between the stress and strain tensors can describe the elastic response. Modeling techniques such as the fast Fourier transform (FFT) based algorithm or finite element modeling (FEM) can be used to compute this relationship and predict the overall and local elastic behavior of the material [1]. However, especially as a result of advanced characterization techniques, the size of the data sets used in these simulations has been growing rapidly. This makes calculations computationally expensive, which provides motivation for defining how large a volume is required in order to obtain accurate predictions of, e.g. micromechanical response. There are studies that define 3D representative volume elements (RVEs) in order to estimate the overall elastic material properties [2, 3], texture evolution [4], phase transformation dynamics [5], and plastic behavior [6] of polycrystalline aggregates through the smallest possible simulation domains. However, these analyses do not extend to examining the effect of grain interactions on the local level elastic field distributions, which is especially crucial in the investigation of critical events such as fatigue crack initiation/growth studies. For instance, Stein *et al* [7, 8] used the elastic FFT method to investigate the stress state in the vicinity of microstructurally small fatigue cracks by simulating the full field anisotropic elastic response using the EBSD maps (in 2D). They reported that the observed cracks are located along coherent $\Sigma 3$ boundaries that are oriented favorably for slip. To further support this finding, the region around one of the identified cracks was characterized using high energy x-ray diffraction microscopy (HEDM) [9, 10] on the 1-ID beamline at the Advanced Photon Source (Argonne National Laboratory). With this characterization technique, the specimen cross sectional diameter is limited to about 1 mm, as detailed in section 3, which meant that only a certain number of grains could be mapped. Thus, it is uncertain whether or not the characterized volume was sufficient to provide enough information for simulations, and if it was, whether it is possible to divide the volume into smaller simulation domains without losing stress/strain resolution for computational efficiency. This uncertainty can be studied by posing the question, 'based on the anisotropic elastic response of the polycrystal, how many neighbor grains are required for stress–strain fields to converge in a chosen grain?', which is a variant of the question, 'How large of a RVE is required in order to study the behavior of a specific location, e.g. the region around the microcrack in a polycrystal?'. As will be detailed in the results section, this question is tested by selecting smaller and smaller volumes from the whole specimen, each of which contains the same identified crack adjacent to a (coherent) twin boundary, the uncertainty or confidence of which is quantified by the Pearson correlation coefficient. By taking the largest down-sampled RVE as the reference state, both voxel

by voxel and mean field comparisons are performed to determine how well-converged each subset domain is to the reference volume. After the simulation size requirement is found for the specific experimental LSHR data, the scope of the analysis is extended to synthetically created, statistically representative structures in order to study the effect of anisotropy, deformation boundary conditions, loading direction, and texture on the local level elastic behavior.

2. Experimental and synthetic microstructures

2.1. Ni-based superalloy, LSHR

Superalloys have superior mechanical performance such as high strength, high oxidation, and high creep and fatigue resistance, even at elevated temperatures. LSHR, a Ni-based, advanced disk superalloy that was developed by NASA researchers [12], was processed and tested at the Air Force Research Laboratory (AFRL) at Wright-Patterson Air Force Base for the fatigue crack initiation study [7, 8, 11]. The samples were manufactured using powder metallurgy, with powder particle diameters constrained to less than about 55 μm. The microstructure in the middle of the gauge section was coarsened at AFRL [13] via localized heat treatment to produce a grain size of approximately 23 μm, whereas the grain size in the fine region was approximately 4 μm. The specimen was cyclically loaded in tension–tension, and the test was interrupted at 37 500 cycles when small cracks were detected on the surface of the specimen. Stein *et al* [7, 8] used scanning electron microscopy (SEM) to characterize the surface of the fatigued specimens, which revealed microcracks on the electropolished surface. Additionally, the region around one of the identified cracks was mapped at Argonne National Laboratory as detailed in section 3. This microstructure was used in the sensitivity analysis shown in figure 2.

2.2. Synthetic structure

To further investigate the convergence, statistically representative microstructures (SRMs) were reconstructed via DREAM.3D, an open-source modular software package that was developed by Groeber and Jackson for the purpose of representing, processing, segmenting, quantifying, and synthesizing microstructures in 3D [14]. With the intention of investigating the effect of loading condition/direction, anisotropy, and texture, a single-phase, equiaxed, cubic structure was constructed on a 315^3 voxel grid. Based on one voxel per μm and an average grain size of 20 μm, the largest domain contained 7515 grains. Two different texture states were assigned to the SRMs: random (figure 1(a)) and preferred (1 0 0) texture (figure 1(b)). Effectively, these two textures represent weak versus strong texture. The issue of sensitivity to general texture variations, which represents a substantial effort, will be addressed in a future work. The reader is referred to Groeber *et al* [15] and the DREAM.3D website [16] for details of statistics generation and the capabilities of the software.

3. Microstructure characterization using HEDM

HEDM is a non-destructive 3D microstructure mapping method, in which monochromatic high energy x-rays from a synchrotron source, in this case the Advanced Photon Source (APS) at Argonne National Laboratory, are used to characterize bulk samples. A brief description of the technique is presented here, but for more detail the reader is directed to Suter *et al*, Hefferan *et al* and Li and Suter [9, 10, 17, 18]

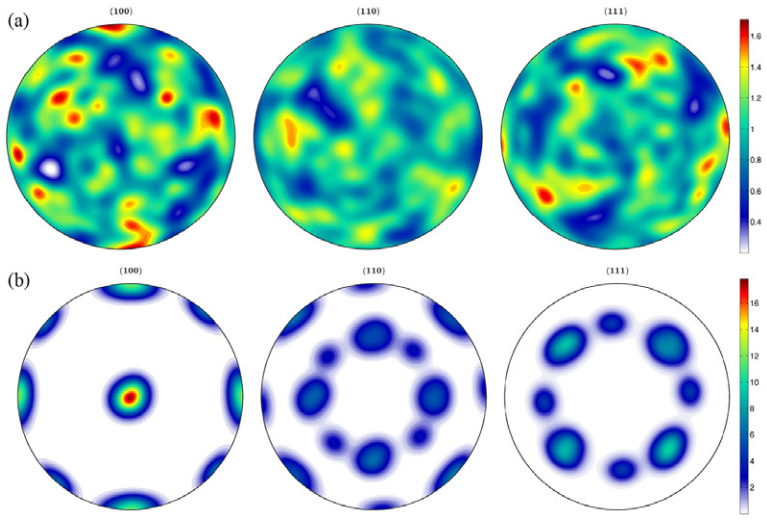

Figure 1. Pole figures showing the crystallographic texture for the synthetically created microstructures: (a) Random texture for loading condition/direction and anisotropy analysis; (b) (1 0 0) fiber texture for analysis of the effect of preferred orientation.

The near-field HEDM experiment involves collection of diffractograms by a high spatial resolution detector, placed 5–10 mm away from a specimen that is centered on a rotation stage. Diffractograms are repeatedly collected from each layer of the specimen as the sample rotates through one-degree increments spanning 180° of rotation [17], with two different stand-off distances for the detector at each rotation position. Reconstruction of the 3D orientation map relies on a forward modeling algorithm, as explained by Suter [9] and Li and Suter [10]. The reconstruction software, IceNine [19], simulates the experiment by creating a sample grid and simulating the diffraction for each voxel for crystal orientations spanning a fundamental zone of orientations for a given symmetry. The simulated diffraction is compared to the actual data and the best fit is selected [9].

A fatigued LSHR sample was characterized with nf-HEDM. The reconstruction provided an image with 0.1° orientation resolution [10]. A total of 61 layers were scanned using a typical 4 μm increment in the z direction between layers; the reconstruction was performed using IceNine with a mesh resolution of 0.923 μm in the x and y directions, figure 2. The full volume contained on the order of 39 million independent orientation measurements and 37 481 grains. As suggested by the variegated orientation color, the texture is random.

After Stein *et al* [8] performed EBSD on the same LSHR sample, the 2D surface orientation map was aligned with the HEDM reconstruction in order to label the crack neighboring grains in the 3D map, as shown in figure 3. Previously Marrow *et al* [20] studied short fatigue crack nucleation via high resolution x-ray tomography and investigated the shape of the MSFC without having the crystallographic information. In another study, Ludwig *et al* [21] simultaneously 3D imaged a short crack and its surrounding crystallographic grains in order to investigate crack propagation. Our LSHR sample and reconstruction differs from these studies in that the existing crack is microstructurally small, i.e. on the order of the grain size, making local neighborhood sensitivity analysis a precursor for the investigation of crack initiation [8].

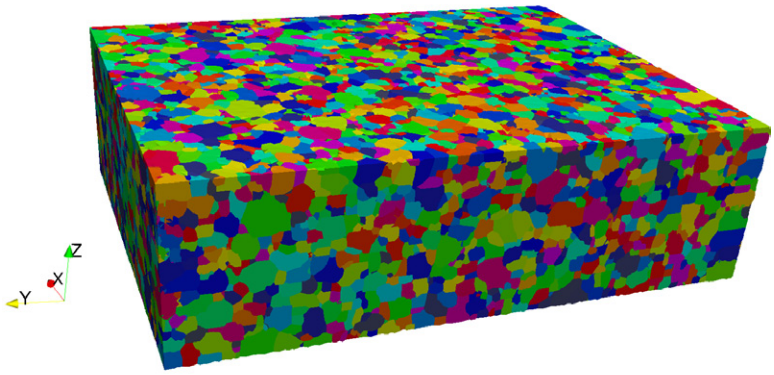

Figure 2. Full reconstructed volume of LSHR from nf-HEDM, with approximate dimensions 600 μm $\times$ 800 μm $\times$ 240 μm. False colors are mapped from the Rodrigues vector components specifying the orientation at each point.

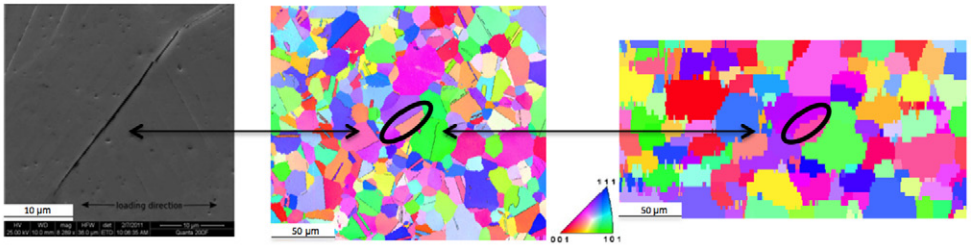

Figure 3. (a) SEM image of the microcrack (rotated to match the reference frame of HEDM) [7] (b) EBSD map of the same region (c) HEDM map of the same region. (Coloring is based on the crystallographic plane exposed at the surface, *aka* inverse pole figure coloration. Spatial resolution and color scaling is different for figures 3(b) and (c)).

4. Fast Fourier transform based modeling

Moulinec and Suquet introduced the FFT formulation as a tool for full-field simulation of the mechanical response. In general, the FFT algorithm computes the stress and strain fields at each point on a grid based on the crystallographic orientation of the point [22]. It uses a microstructural image with orientation information as direct input, and requires periodic unit cells and boundary conditions. Since the method does not require meshing, the calculation is computationally efficient and able to manage a large number of degrees of freedom typically involved in the description of complex microstructures [23]. The reader is directed to Moulinec and Suquet [22], and Lebensohn [23–25] for detailed explanations of the method.

To the authors' knowledge, an analysis of the FFT method to determine the minimum grain neighborhood required to obtain converging local field distribution has not yet been reported. In other words, it is unknown whether or not one should expect the local mechanical behavior within a chosen grain to relate to one another when the simulation representative volume element (RVE) size changes. Examining the local distribution sensitivity can help define the RVE selection process. Depending on the results, elastic FFT can be categorized as a method that requires one to use the full microstructure volume in the simulations to get correct results,

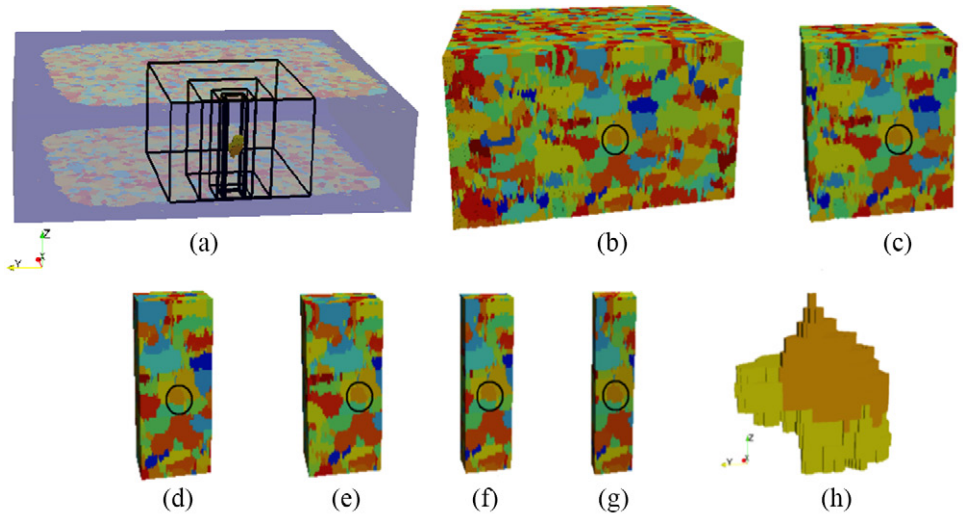

Figure 4. (a) Full image, crack neighbor surface grains and the outline of the sub domains. RVEs with domain sizes of (b) $512 \times 512 \times 64$ (c) $256 \times 256 \times 64$ (d) $128 \times 128 \times 64$ (e) $121 \times 121 \times 64$ (f) $81 \times 81 \times 64$ (g) $64 \times 64 \times 64$ (h) Crack neighbor grains. The color is based on the orientation via the Rodrigues parameters.

or allows one to use subset regions of interest from the entire volume, which would still give correct results in a computationally more efficient manner. Given that the FFT method solves the same full field micromechanical response as does the finite element method, the same considerations are expected to apply to the latter.

5. LSHR results and discussion

The near field HEDM reconstruction of the LSHR sample is used as direct input for this study. As stated in section 1, the question is, 'How many neighbor grains are required for stress–strain fields to converge in a chosen grain?' Positioning the identified crack neighbor surface grains at the center of the images, six RVEs are subdivided out of the full volume, where the largest one with the domain size of $512 \times 512 \times 64$ is used as reference in the comparisons. Since the resolution of HEDM is lower at the surfaces, an optimized cut plane is applied to discard poorly indexed surface voxels. To preserve the periodicity that is required in the FFT calculations, the unit cell surfaces are covered with four voxels of buffer layers in the x and y directions. Then the original 61 z-layers of the HEDM scan is completed to 64 layers by mirroring the bottom three layers to the top in the loading, z, direction in order to have 2^n z-dimensions for parallel decomposition of the problem. Figure 4 shows the structures used in simulations where the identified cracked region is circled for each case, along with the magnified crack neighbor grains.

The elastic stiffness components are chosen as $C_{11} = 247\,\text{GPa}$, $C_{12} = 155\,\text{GPa}$, and $C_{44} = 125\,\text{GPa}$, in line with the experimental data and LSHR mechanical property characterization report [12], giving an anisotropy factor of 2.71. The strain boundary condition is chosen as $\varepsilon_1 = \varepsilon_2 = -0.000\,86$ and $\varepsilon_3 = 0.003$ since it is a simulation of tension in the z direction with a Poisson's ratio of 0.286. For each RVE, identical strain boundary conditions and elastic coefficients are used to simulate elastic tension.

Table 1. Number of grains per volume in each simulation domain based on the experimentally measured volume, together with the average stress and strain values for the crack neighbor grains.

		512 × 512 × 64	256 × 256 × 64	128 × 128 × 64	121 × 121 × 64	81 × 81 × 64	64 × 64 × 64
	Number of grains	11780	3114	875	738	356	257
Max principal strain (mm mm^{-1})	Lower grain	0.0027	0.0027	0.0027	0.0027	0.0027	0.0027
	Upper grain	0.0036	0.0036	0.0036	0.0036	0.0036	0.0036
Max principal stress (MPa)	Lower grain	634.77	634.79	635.92	632.46	629.44	630.69
	Upper grain	626.55	627.10	627.83	623.70	622.29	624.94

The mean values of maximum principal stress and strain for the two crack neighboring grains are shown in table 1. These simulation domains were all based on the experimentally measured (HEDM) volume.

The results presented in table 1 are plotted to visualize the convergence trend as a function of the number of grains included in the simulation subset domains (RVE), figure 5. As frequently noted in the literature, of the crack neighbor grains, one grain is stiffer than the other [26] so it has a higher stress but a lower strain. Figure 6 shows the maximum principal stress distributions within the two grains of interest.

In agreement with the convergence trend observed with mean values, the visualization of the local stress distribution in the two grains, figure 6, also suggests good correlation. To demonstrate this quantitatively, voxel by voxel results are compared between the largest (reference) volume and each of the other volumes in turn. Pearson correlation coefficients are presented for maximum principal stress of the crack neighbor grains in table 2.

Quantitative voxel by voxel comparison shows that for a correlation larger than 99%, 356 or more grains must be present in the simulation domain. For the LSHR specimen, the convergence trend is observed for 81 × 81 × 64 and larger grids, as depicted in the following correlation plots, figure 7. This result of the sensitivity analysis shows that for the elastic FFT calculation, stress–strain distributions are not very sensitive to the shape of the domain. It is not mandatory to use the entire sample in the simulations, and computation time can be decreased substantially by trimming smaller volumes that contain the region of interest.

6. Synthetic results and discussion

First, the anisotropy factor effect on convergence is examined with a random texture SRM. The maximum domain is trimmed to voxel dimensions 225^3 (3156 grains), 128^3 (657 grains), 121^3 (613 grains), 81^3 (205 grains) and 64^3 (112 grains) on two different configurations; one set having a shared surface and one set sharing the origin at the center. The structures are covered with four voxels of buffer layers on each side, and three grain pairs from various locations are chosen for convergence study. Figure 8 shows the structures, subdomains, and grain pairs of interest with random and preferred textured structures.

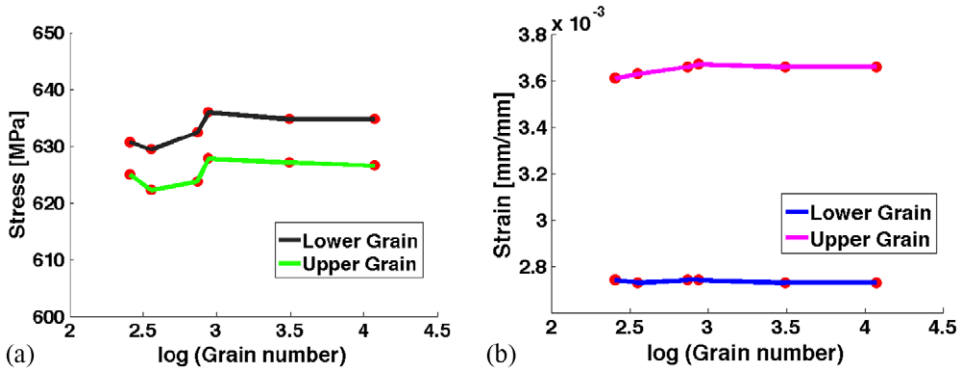

Figure 5. (a) Average maximum principal within the crack neighbor grains as a function of the number of grains in the RVE; (b) average max principal strain within the crack neighbor grains versus the log of number of grains in the RVE.

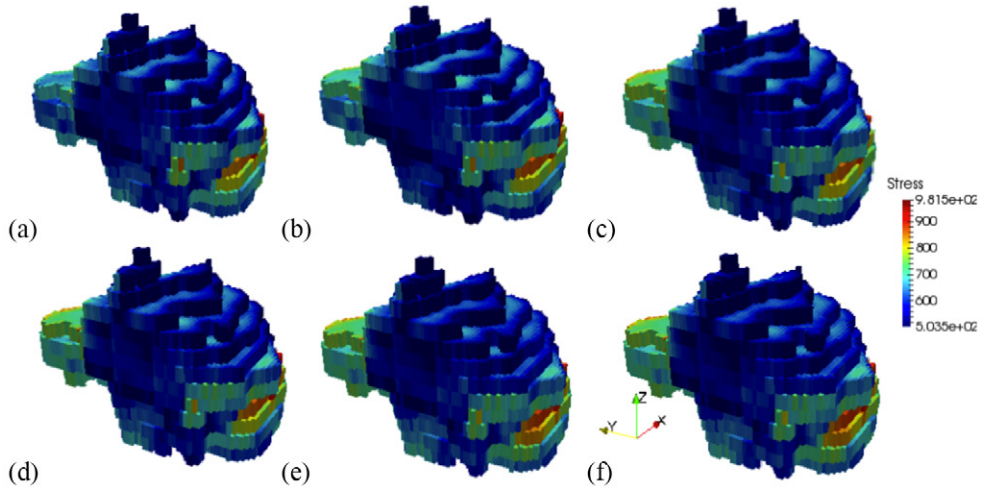

Figure 6. Max principal stress distributions for two neighbor grains around the identified microcrack for RVE of (a) $512 \times 512 \times 64$ (b) $256 \times 256 \times 64$ (c) $128 \times 128 \times 64$ (d) $121 \times 121 \times 64$ (e) $81 \times 81 \times 64$ (f) $64 \times 64 \times 64$. The stress values are rescaled with respect to the largest RVE for comparison.

The effect of anisotropy is investigated on one grain pair through the use of Ni elastic properties (section 5), Cu elastic properties ($C_{11} = 168\,\text{GPa}$, $C_{12} = 122\,\text{GPa}$, $C_{44} = 75\,\text{GPa}$ corresponding to an anisotropy factor of 3.26), and Al elastic properties ($C_{11} = 106\,\text{GPa}$, $C_{12} = 60\,\text{GPa}$, $C_{44} = 28\,\text{GPa}$ corresponding to an anisotropy factor of 1.22). Stress distributions in figure 9 and the Pearson correlation coefficient values presented in table 3 indicate that as the anisotropy increases, the correlation decreases; however, it is still possible to find convergence in terms of the number of grains. In the case of Al, it is found that even 64^3 is large enough for both the lower and upper grains to exhibit a Pearson's correlation coefficient of $\geqslant 99$ %, whereas for Cu, having higher anisotropy, 81^3 is large enough for the lower grain and 128^3 is large enough for the upper grain. Taking anisotropy and the shape of the domain into account, it is concluded that if there is a region of interest, one should include at least to the third nearest neighbor in the simulations.

Table 2. Pearson correlation coefficients for max principal stress values within the two grains neighboring the crack.

	512 versus 64	512 versus 81	512 versus 121	512 versus 128	512 versus 256
Lower grain, stress	0.96	0.99	0.99	0.99	0.99
Upper grain, stress	0.97	0.99	0.99	0.99	0.99

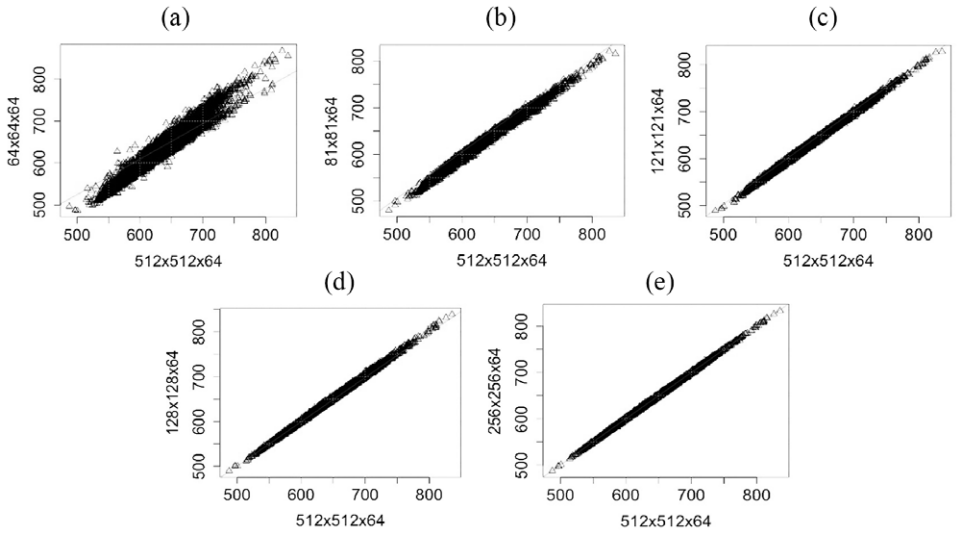

Figure 7. Lower grain maximum principal stress correlation plots between values for the reference volume 512 × 512 × 64 on the *x*-axis and values for (a) 64 × 64 × 64, (b) 81 × 81 × 64, (c) 121 × 121 × 64, (d) 128 × 128 × 64, (e) 256 × 256 × 64 on the *y*-axis.

The effect of loading direction is examined by imposing 0.5 % tension strain along the *x*, *y*, and *z* directions on the randomly textured SRMs with Ni elastic properties. For both bulk and surface grains, it is found that for uniaxial *x* (figure 10(a)), *y* (figure 10(d)) and *z* (figure 10(f)) loadings, 121^3 domain size is enough to obtain $R \geqslant 99$ %. A similar trend is observed as the loading condition is changed to combinations of biaxial tension and compression in different directions; convergence is again found on the 121^3 grid (figures 10(b), (c) and (g),). The assigned texture is found to be the most influential parameter on the sensitivity, especially when the loading is parallel to the preferred orientation (figures 10(h) and (i). For the case of the (1 0 0) preferred texture and tensional x loading along texture fiber, only the largest subset 225^3 having 3156 grains, is found to be sufficient for $R \geqslant 99$ %. Pearson correlation coefficients for the combinations of loading state and texture are given in table 4.

7. Conclusion

The size, anisotropy, loading condition, loading direction, and texture dependence study reported here indicates that the elastic calculation is rather insensitive to the domain size, provided that a few shells of the nearest neighbor grains are included. Taking the shape of the domains into account, it is concluded that an RVE can be determined around the region of interest for the local elastic calculations. This provides the researcher the opportunity to map

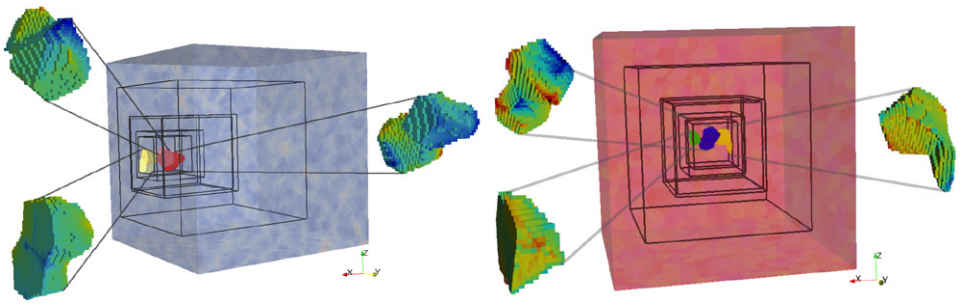

Figure 8. RVEs and investigated grain pairs based on the synthetic microstructures: On the left is for the loading condition/direction and anisotropy analysis and on the right is for the texture analysis.

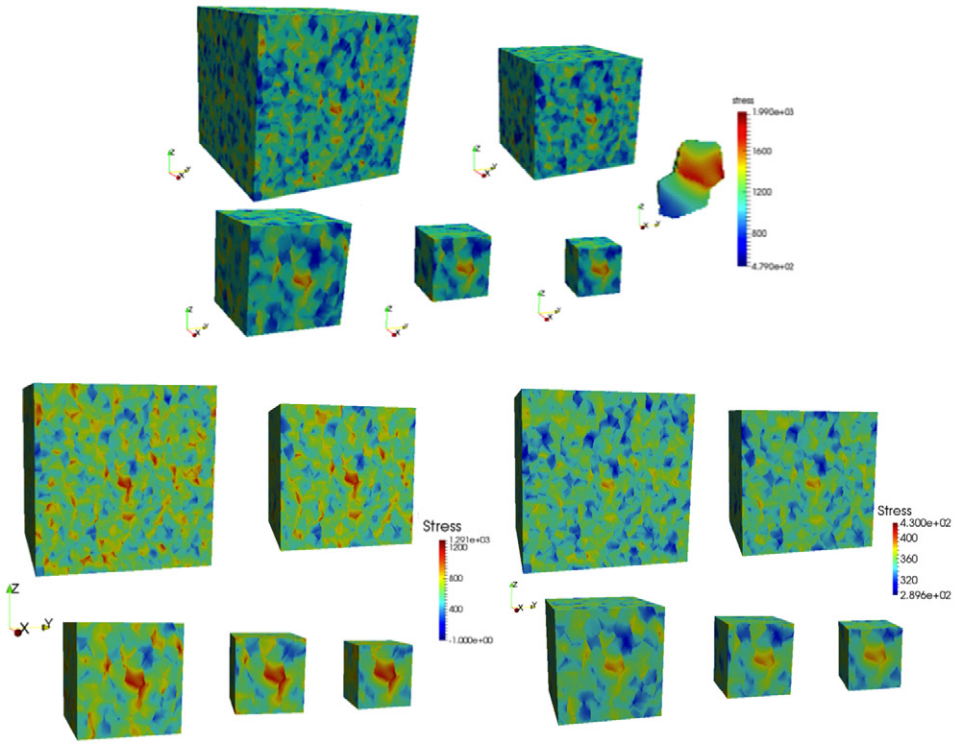

Figure 9. Maximum principal stress distributions per domain (315^3, 225^3,128^3, 81^3 and 64^3) for Ni elastic anisotropy parameters on the top, Cu on the bottom left and Al on the bottom right.

small microstructure regions as in the case of HEDM. Based on the results of the full field elastic FFT calculations on randomly oriented materials with anisotropy factor smaller than 3.26, the local and average mechanical fields are found to be insensitive to the size of the volume when equal to or more than the third nearest neighbor grains are included in the simulation. For the LSHR analysis this corresponds to 356 total grains in a grid of size $81 \times 81 \times 64$ voxels, and for the synthetic structures with 613 total grains in a grid of size 121^3. However,

Table 3. Pearson correlation coefficients for anisotropy based on Cu, Ni and Al.

		315 versus 64	315 versus 81	315 versus 128	315 versus 225
Cu ($f = 3.26$)	Lower grain, stress	0.98	0.99	0.99	0.99
	Upper grain, stress	0.97	0.98	0.99	0.99
Ni ($f = 2.71$)	Lower grain, stress	0.98	0.99	0.99	0.99
	Upper grain, stress	0.97	0.99	0.99	0.99
Al ($f = 1.22$)	Lower grain, stress	0.99	0.99	0.99	0.99
	Upper grain, stress	0.99	0.99	0.99	0.99

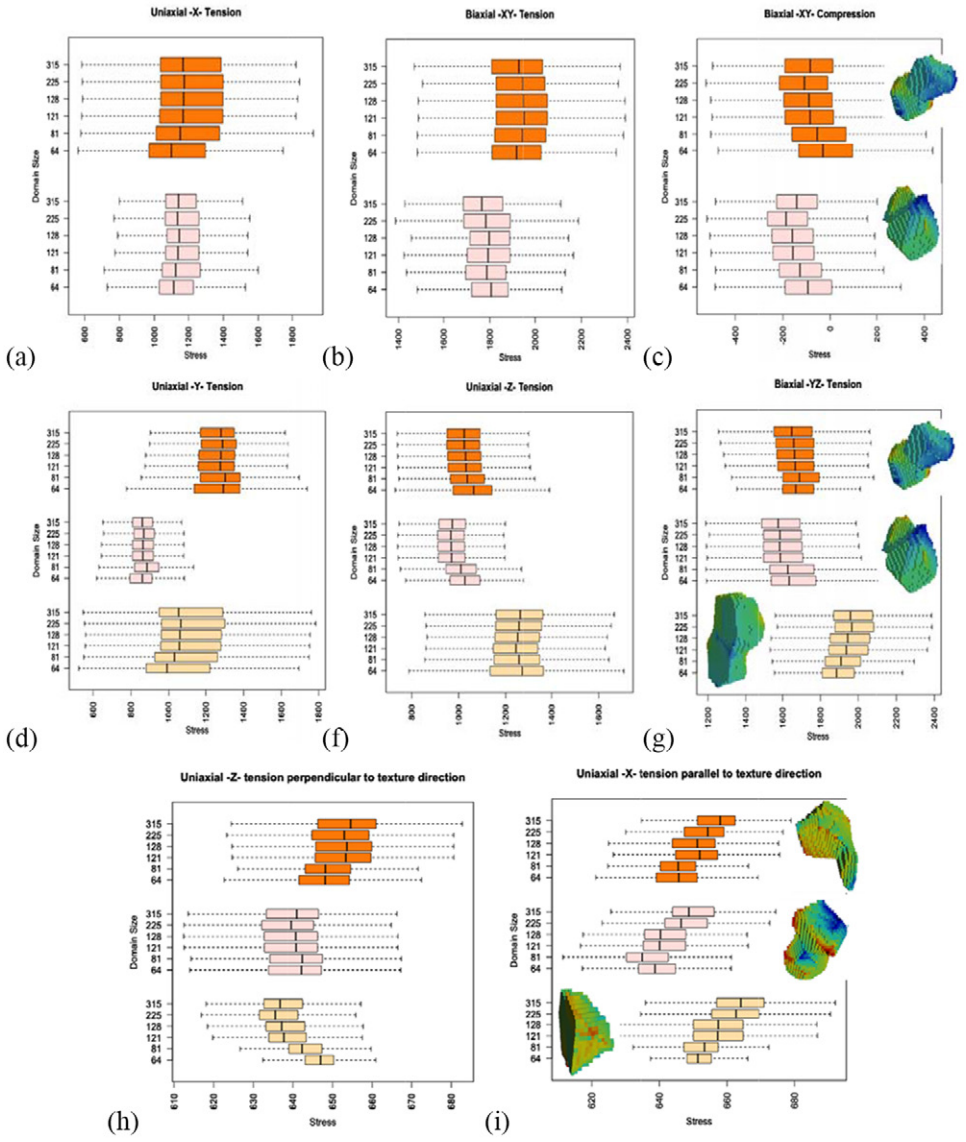

Figure 10. Box plots showing the effect of (a) loading direction (b) loading condition (c) texture on the domain size sensitivity.

Table 4. Pearson correlation coefficients based on the loading direction, loading condition and texture analyses.

		315 versus 64	315 versus 81	315 versus 121	315 versus 128	315 versus 225
X tension	Pair 1	0.97	0.98	0.99	0.99	0.99
	Pair 2	0.97	0.99	0.99	0.99	0.99
XY tension	Pair 1	0.92	0.96	0.99	0.99	0.99
	Pair 2	0.97	0.99	0.99	0.99	0.99
XY compression	Pair 1	0.93	0.96	0.99	0.99	0.99
	Pair 2	0.92	0.97	0.99	0.99	0.99
Y tension	Pair 1	0.98	0.99	0.99	0.99	0.99
	Pair 2	0.95	0.96	0.99	0.99	0.99
	Pair 3	0.97	0.99	0.99	0.99	0.99
Z tension	Pair 1	0.98	0.99	0.99	0.99	0.99
	Pair 2	0.96	0.98	0.99	0.99	0.99
	Pair 3	0.95	0.98	0.99	0.99	0.99
XZ tension	Pair 1	0.97	0.98	0.99	0.99	0.99
	Pair 2	0.97	0.98	0.99	0.99	0.99
	Pair 3	0.96	0.99	0.99	0.99	0.99
Z tension perpendicular to texture fiber	Pair 1	0.89	0.96	0.98	0.99	0.99
	Pair 2	0.97	0.98	0.99	0.99	0.99
	Pair 3	0.96	0.99	0.99	0.99	0.99
X tension along texture fiber	Pair 1	0.93	0.93	0.97	0.98	0.99
	Pair 2	0.97	0.93	0.96	0.97	0.99
	Pair 3	0.97	0.98	0.97	0.98	0.99

the texture effect should be considered carefully when combined with the loading conditions and directions.

Acknowledgments

Partial support by AFOSR Discovery Challenge Thrust grant #FA9550-10-1-0213 is acknowledged. The research was also supported in part by the National Science Foundation through TeraGrid resources provided by Texas Advanced Computing Center under grant number DMR080072. Use of the Advanced Photon Source was supported by the US Department of Energy, Office of Science, Office of Basic Energy Sciences, under Contract No DE-AC02-06CH11357. The authors are grateful to Dr Jonathan Lind for his contribution in collecting and analyzing the HEDM data, and also his algorithms for segmentation of diffractograms, which greatly facilitated the reconstruction. The authors are grateful to Dr S L Semiatin for heat treating the LSHR specimens to produce the coarse microstructure and Mr W John Porter (University of Dayton Research Institute) for microstructural characterization.

References

[1] Ghosh S and Dimiduk D 2011 *Computational Methods for Microstructure-Property Relationships* vol 1 (New York: Springer) pp 199–238, 393–441
[2] Gusev A A 1997 Representative volume element size for elastic composites: a numerical study *J. Mech. Phys. Solids* **45** 1449–59

[3] Kanit T *et al* 2003 Determination of the size of the representative volume element for random composites: statistical and numerical approach *Int. J. Solids Struct.* **40** 3647–79
[4] Ammar K, Appolaire B, Cailletaud G and Forest S 2009 Combining phase field approach and homogenization methods for modelling phase transformation in elastoplastic media *Eur. J. Comput. Mech.* **18** 485–523
[5] Nakamachi E, Tam N N and Morimoto H 2006 Multi-scale finite element analyses of sheet metals by using SEM-EBSD measured crystallographic RVE models *Int. J. Plast.* **23** 450–89
[6] Boyle K P and Curtin W A 2005 Grain interactions in crystal plasticity *NUMISHEET 2005* vol 778 pp 433–8
[7] Stein C, Lee S and Rollett A 2012 An analysis of fatigue crack initiation using 2D orientation mapping and full-field simulation of elastic stress response *Superalloys 2012* (Hoboken, NJ: Wiley)
[8] Stein C *et al* 2014 Fatigue crack initiation, slip localization and twin boundaries in a nickel-based superalloy *Curr. Opin. Solid State Mater. Sci.* **18** 244–52
[9] Suter R M *et al* 2006 Forward modeling method for microstructure reconstruction using x-ray diffraction microscopy: single-crystal verification *Rev. Sci. Instrum.* **77** 123905
[10] Li S F and Suter R M 2013 Adaptive reconstruction method for three-dimensional orientation imaging *J. Appl. Crystallogr.* **46** 512–24
[11] Cerrone A *et al* 2015 Implementation and verification of a microstructure-based capability for modeling microcrack nucleation in LSHR at room temperature *Modelling Simul. Mater. Sci. Eng.* **23** 035006
[12] Gabb T P *et al* 2005 Thermal and mechanical property characterization of the advanced disk alloy LSHR *NASA/T*, 2005–213645
[13] Semiatin S L, Air Force Research Laboratory, Materials and Manufacturing Directorate, Wright-Patterson AFB, OH 45433. Unpublished results
[14] Groeber M and Jackson M 2014 DREAM.3D: a digital representation environment for the analysis of microstructure in 3D *Integr. Mater. Manuf. Innov.* **3** 5
[15] Groeber M, Ghosh S, Uchic M D and Dimiduk D M 2008 A framework for automated analysis and simulation of 3d polycrystalline microstructures: II. Synthetic structure generation *Acta Mater.* **56** 1257–73
[16] Groeber M and Jackson M 2014 DREAM.3D, Version 4.2.4920 [Software] Available from http://dream3d.bluequartz.net/index.html
[17] Suter R M *et al* 2008 Probing microstructure dynamics with x-ray diffraction microscopy *J. Eng. Mater. Technol.* **130** 021007
[18] Hefferan C *et al* 2012 Observation of recovery and recrystallization in high purity aluminum measured with forward modeling analysis of high energy diffraction microscopy *Acta Mater.* **60** 4311–8
[19] Li S F 'IceNine' https://github.com/FrankieLi/IceNine
[20] Marrow T J *et al* 2004 High resolution x-ray tomography of short fatigue crack nucleation in austempered ductile cast iron *Int. J. Fatigue* **26** 717–25
[21] Ludwig W, Buffiere J-Y, Savelli S and Cloetens P 2003 Study of the interaction of a short fatigue crack with grain boundaries in a cast Al alloy using x-ray microtomography *Acta Mater.* **51** 585–98
[22] Moulinec H and Suquet P 1998 A numerical method for computing the overall response of nonlinear composites with complex microstructure *Comput. Methods Appl. Mech. Eng.* **157** 69–94
[23] Lebensohn R A 2001 'N-site modeling of a 3D viscoplastic polycrystal using fast Fourier transform *Acta Mater.* **49** 2723–37
[24] Lebensohn R A *et al* 2004 On the accuracy of the self-consistent approximation for polycrystals: comparison with full-field numerical simulations *Acta Mater.* **52** 5347–61
[25] Lebensohn R A *et al* 2012 An elasto-viscoplastic formulation based on fast Fourier transforms for the prediction of micromechanical fields in polycrystalline materials *Int. J. Plast.* **32** 59–69
[26] Miao J, Pollock T M and Wayne Jones J 2009 Crystallographic fatigue crack initiation in nickel-based superalloy René 88DT at elevated temperature *Acta Mater.* **57** 5964–74